Revista Brasileira de Farmacognosia (2024) 34:522–535
https://doi.org/10.1007/s43450-023-00501-8

ORIGINAL ARTICLE

# Isoflavone-Rich Extract of *Trifolium resupinatum*: Anti-obesity Attributes with *In Silico* Investigation of Its Constituents

**Mona M. Marzouk[1] · Alia Y. Ragheb[1] · Elham M. Youssef[2] · Nermin A. Ragab[3] · Eman M. El-Taher[4] · Ibrahim A. El Garf[5] · Mona E. S. Kassem[1]**

Received: 2 June 2023 / Accepted: 23 November 2023 / Published online: 2 January 2024


## Abstract

*Trifolium resupinatum* L., Fabaceae, aqueous methanol leaf extract was selected to mitigate some obesity-associated risk factors to validate the possibility of further developing herbal drugs. Chromatography and spectrophotometric techniques verified 14 phenolics, five of which were first isolated from the plant and identified as 6''-*O*-acetyl ononin, genistin, daidzin, sissotrin, and astragalin. Further phytochemical characterization was performed via liquid chromatography-electrospray ionization-mass spectrometry assisted by a spectral similarity molecular network. In total, 81 metabolites were tentatively annotated including 69 species-first dereplications. Two major isolates (formononetin and pseudobaptigenin) were selected along with the investigated extract for an *in vitro* pancreatic lipase inhibition assay. They showed notable effects with $IC_{50}$ values (µg/ml): 47.2 ± 1.1, 112.8 ± 1.23, and 471.32 ± 0.8, respectively, incomparable to orlistat (23.8 ± 0.64). Preliminary *in vivo* assay (25 mg/kg extract, daily, 8 weeks) displayed weight loss interest and promising advancement of serum triacylglycerides, total cholesterol, and glucose levels. Molecular docking studies confirmed the promising binding score of formononetin and pseudobaptigenin near the active sites and highlighted the affinity of other isolates to the lipase enzyme. Several isolates passed Lipinski's law of the drug-likeness test, whereas SwissADME radar displayed that all constituents fall within the acceptable bioavailability zone. Therefore, the combination of flavonoids, especially isoflavones, could be regarded as drug-like agents for protection against obesity-induced metabolic complaints.

**Keywords** Computational analysis · High-fat diet · LC-ESI-MS · Natural compounds · Persian clover

## Introduction

Being overweight increases the chances of developing serious complications such as diabetes mellitus (type II), cardiovascular disorders, osteoarthritis, some types of cancer, and stroke. Obesity reflects both genetic and acquired correlated factors and contributes to dyslipidemia (high LDL cholesterol, high triacylglyceride, and low HDL cholesterol levels), insulin resistance or impaired blood glucose, and borderline hypertension (Sarma et al. 2021). Glycolipid metabolism abnormalities can be said to affect about 12.5 to 31.4% of the population of most countries and are expected to keep rising as obesity rates increase. One billion people are expected to be obese worldwide by 2030 (Noubiap et al. 2022). Besides, higher medical treatment expenses would be incurred as many complications are present. A long-term lifestyle regimen begins with weight loss (low-fat diet) and modifying physical activity enhances metabolic symptoms but not to a sufficient

✉ Mona M. Marzouk
mm.marzouk@nrc.sci.eg

1 Department of Phytochemistry and Plant Systematics, National Research Centre, 33 El Bohouth St., P.O. 12622, Cairo, Egypt

2 Department of Biochemistry, National Research Centre, 33 El Bohouth St., P.O. 12622, Cairo, Egypt

3 Department of Pharmacognosy, National Research Centre, 33 El Bohouth St., P.O. 12622, Cairo, Egypt

4 Department of Pharmacognosy, Faculty of Pharmacy, Egyptian Russian University, P.O. 63514, Badr City, Cairo, Egypt

5 Department of Botany and Microbiology, Faculty of Science, Cairo University, P.O. 12613, Giza, Egypt

degree. The complicated treatment plan involves several different medications which result in drug interactions, side effects, and an insufficient therapeutic response. Therefore, searching through food components and developing new medications with diverse activities is one prospective approach (Lillich et al. 2021).

In the modern era, computational drug design is one of the key mechanisms for pharmaceutical discovery. The rapid advancement of new drugs is significantly assisted by molecular docking studies. Additionally, molecular modeling projections validate the outcomes of molecular docking (Al-Karmalawy et al. 2021). Innovative in silico approaches, such as molecular docking, are utilized to highlight the interactive mechanism between targeted obesity-related enzymes and their potential inhibitors. Therefore, it provides an influential, coherent, and low-cost implementation for the screening of novel bioactive natural compounds (de Lima Barros et al. 2022). Nowadays, bioinformatics and combinatorial chemistry are the most dynamic approaches to find potent druggable candidates in the drug-development field (Swain and Hussain 2022).

*Trifolium* L. (clover or trefoil) is an important economic genus of the family Fabaceae (Leguminosae), consisting of approximately 300 species from the Mediterranean area, temperate, and somewhat subtropical regions of North and South America. *Trifolium* species are high-protein fodder plants eaten by cattle and wildlife, and indirectly improve human health (Kassem et al. 2017). In addition, clovers have a long history of being valued as remedial plants for curing various skin, respiratory, nervous, reproductive, and digestive complaints (Kolodziejczyk-Czepas 2016). In recent years, numerous therapeutic effects have been supported concerning their traditional uses as antioxidant, anti-inflammatory, antihyperglycemic, anticancer, antimicrobial, hepatoprotective, and healing effects (Malca-Garcia et al. 2022). Moreover, the estrogenic effect of clovers was proven to alleviate menopausal symptoms and serve as an alternative therapy for disorders associated with metabolic syndrome (Jungbauer and Medjakovic 2014). Lately, the ameliorated impact of *Trifolium pratense* L. (red clover) isoflavones extract against metabolic syndrome elements was proved by Yokoyama et al. (2020). Likewise, its extract significantly improved the plasma lipid profile after menopause, decreased plasma glucose levels, and increased insulin sensitivity in diabetic rats (Oza and Kulkarni 2020). *Trifolium resupinatum* L. (Persian or Reversed clover) is indigenous to the Mediterranean, southern Europe, and southwest Asia (Singh et al. 2019). It is one of the economically valuable pasture crops popularly used as fodder and hay for livestock. In Egypt, this species grows densely along the Nile River, irrigation canals, and drainage networks. It is considered an aggressive species because it quickly spreads to cover any exposed soil (Elkordy et al. 2019). Previous works on the aerial parts of *T. resupinatum* characterized the high levels of isoflavone and flavonol metabolites (Kassem et al. 2017).

In the present research, phenolic compounds were isolated from the aqueous methanol *T. resupinatum* leaf extract and used them as standards with other reference phenolics through the LC-ESI-MS/MS analysis. Global natural products social (GNPS)-based molecular networking was integrated. Two major isoflavone isolates along with the investigated extract were examined for their ability to suppress pancreatic lipase *in vitro*. The other isolates were virtually screened through molecular docking, which is conceivably the implicit mechanism of preventing obesity caused by the suppression of pancreatic lipase. In addition, the extract was checked for its effect on the development of some metabolic syndrome criteria in a high-fat diet-induced obese rat model. The isolated compounds were also assessed for absorption, distribution, metabolism, and excretion (ADME), as well as for drug-likeness.

## Material and Methods

### General Procedures

The ultraviolet analyses were recorded at Shimadzu UV-240 spectrophotometer, and NMR spectra were carried out using Jeol EX-500 spectrometer ($^1$H NMR, 500 MHz). EI-MS data were carried out on a Finnigan-Mat SSQ 7000 spectrometer. A LC-ESI-MS/MS spectrometer was used for MS analysis (negative mode) with an Exion LC AC system for separation and SCIEX Triple Quad 5500 + MS/MS system equipped with electrospray ionization for detection. Polyamide 6S (Flucka, 5 × 140 cm) and Sephadex LH-20 (Pharmazia, Uppsala, Sweden, 2 × 60 cm) column chromatography (CC) and Whatman No. 1 and 3MM paper chromatography sheets (PC) (Whatman Ltd., England, 46 × 57 cm) were used for sample isolation. Methanol, distilled water, acetic acid, and *n*-butanol solvents (Adwic, Cairo, Egypt) with systems: 15% acetic acid ($H_2O$: HOAc, 85:15) and BAW (*n*-butanol:acetic acid:$H_2O$, 4:1:5, upper phase) were applied. Acid hydrolysis was carried out using 2 N HCl for 2 h at 100 °C. For sugar analysis, sugar reference samples (E. Merck, Darmstadt, Germany), and the upper phase of $C_6H_6$-*n*-BuOH-$H_2O$-pyridine (1:5:3:3) solvent system were used, then the PC was sprayed with aniline phthalate reagent. Phenolic acids and flavonoid reference aglycones (isoflavones, flavones, and flavonols) (Fluka AG, Bucns SG, Switzerland) were used for co-PC and LC-MS/MS authentication. A rotary evaporator (HEIDOLPH 4000, Germany) and distiller (Hamilton, Westwood Industrial Estate) were used

for laboratory work. Centrifuge (Sigma 2-15, Germany). The Egyptian Company for biotechnology (S.A.E.) supplied the biochemical spectrum kits, Obour City, Cairo, Egypt.

## Plant Material

*Trifolium resupinatum* L., Fabaceae, was collected and authenticated by Prof. Dr. Ibrahim El Garf from the Botanical Garden of Cairo University. A plant voucher (accession No. 446) was kept at the National Research Centre Herbarium, Giza, Egypt. About 800 g of air-dried leaves powder was extracted by repeated percolation with 70% aqueous methanol (3 × 4 l) and approximately 120 g was yielded after evaporation of the solvent at 60 °C under reduced pressure. Part of the extract (10 g) was set aside to examine its pancreatic lipase inhibitory effect and *in vivo* investigations.

## Chemical Profiling

### Isolation and Structural Elucidation

The remaining residue (110 g) was defatted using chloroform to produce a defatted residue (90 g) which was loaded on a polyamide CC (450 g). Successive elution was carried out starting with water, then the polarity decreased by increasing the methanol in water to 100% methanol. Based on PC properties after spraying with $AlCl_3$ and $FeCl_3$, similar ones were combined, and four main fractions were obtained (A–D). Fraction A ($H_2O$: MeOH; 3:2) (17.2 g) was applied on PC using BAW three times to produce compounds **1** (12 mg), **12** (12 mg), and **14** (18 mg). While fraction B (28.5 g) ($H_2O$: MeOH; 1:1) was purified through 15% acetic acid (double solvent) on PC revealing two subfractions BI and BII. BI (13.8 g) was further chromatographed through Sephadex CC using $H_2O$:MeOH (1:1) eluent and yielded compounds **2** (34 mg), **5** (49 mg), and **7** (8 mg). Likewise, compounds **3** (28 mg), **4** (10 mg), and **8** (10 mg) were isolated from BII (9.5 g). Furthermore, the isolates **6** (23 mg), **9** (10 mg), and **10** (6 mg) were obtained through PPC using BAW followed by 15% acetic acid from fraction C ($H_2O$:MeOH; 3–4:6–7) (12.5 g). Finally, fraction D ($H_2O$:MeOH; 1:4) (7 g) was subjected to PPC using BAW to give **11** (13 mg) and **13** (8 mg) which were eluted through Sephadex CC with $H_2O$:MeOH (1:1) solvent. Repeated purification using Sephadex CC (MeOH) for each sample was achieved.

### LC-ESI-MS/MS Analysis

The analysis was performed using C-18 Column (Ascentis® Express 90 Å, 2.1 × 150 mm, 2.7 µm). Two mobile phases gradient (A: ammonium formate; 5 mM, pH 8 and B: acetonitrile; HPLC grade) were designed as follows: 0–1 min (5% B), 1–20 min (5–100% B), 20.01–25 min (100% B), 25.01–30 min (5% A). The volume (5 µl) was injected and run with a flow rate (0.3 ml/min). The MS/MS negative ionization mode analysis was practical from 100 to 1000 Da with a scan (EMS-IDA-EPI) for MS1 using the ensuing criteria: 25 psi curtain gas, −4500 ion spray voltage, 500 °C source temperature, 45 psi ion source gas 1 and 2, and from 50 to 1000 Da for MS2 with −80 declustering potential, −35 collision energy, and 15 collision energy spread. Negative ionization mode is a useful tool for structural investigations of flavonoids, *i.e.*, through the identification of fragments of interest and relative intensities of some diagnostic ions (Farid et al. 2022). The peaks and spectra were administered using the Analyst TF 1.7.1 and PeakView® 1.2 Softwares (SCIEX, Framingham, MA, USA). The isolated pure compounds were used as standard samples together with other authentic isoflavones and previously isolated phenolics (Marzouk et al. 2012; El Shabrawy et al. 2014; Hussein et al. 2017, 2018; Kassem et al. 2017; El-Sherei et al. 2018). Compounds annotation was assessed by comparing their mass spectrometry data and retention time of each and mapping them through molecular networking.

## Molecular Networking

The molecular network was constructed on the GNPS website (http://gnps.ucsd.edu). Raw data was converted by MSConvert package (Proteowizard Software Foundation, Version 3.0.19330, USA) to an open-source format (.mzML). Using WinSCP (SFTP, FTP, WebDAV and SCP client), the transformed ".mzML" files were uploaded on the GNPS platform. For the comparison of *T. resupinatum* extract and the standard mixtures, the converted data of both were proposed with two groups in one job. GNPS parameters are minimum-matched fragments (four ions), fragment ion tolerance (0.5 u), minimum pairs cosine score (0.65), parent mass tolerance (2.0 u), library search minimum-matched peaks (4), and score threshold (0.65), and do not filter in all library filtering option and other advanced options are set as default. The designed negative molecular network can be retrieved via the following link: https://gnps.ucsd.edu/ProteoSAFe/status.jsp?task=9915465576554c3eb5116d062177ea58. The spectral network was visualized in conjunction with the help of Cytoscape 3.9.1. The molecular networks visualization characterizes each spectrum as a node, and spectrum-to-spectrum groupings as edges and associated by structural correspondence identified via the MS (Xu et al. 2021). Natural products dereplication databases were also searched such as ChemSpider (http://www.chemspider.com/) PubChem (https://pubchem.ncbi.nlm.nih.gov/) and Dictionary of Natural Products (http://dnp.chemnetbase.com/faces/chemical/Chemical Search.xhtml).

## Biological Assessment

### Pancreatic Lipase Inhibition

The porcine pancreatic lipase (PPL) inhibition potential of *T. resupinatum* leaf extract and the two major compounds (**2** and **5**) were established by the *in vitro* method suggested by Kim et al. (2010) using NPB (*p*-nitrophenyl butyrate) as a substrate. A potassium phosphate buffer (0.1 mM, pH 6) was used for the preparation of a lipase solution (100 µg/ml). Samples with different concentrations (7.81–1000 µg/ml) were pre-incubated with lipase solution (10 min, 37 °C) and then the reaction was taking place by addition NPB substrate (0.1 ml), and incubated at 37 °C for 15 min. Finally, a multiplate reader was used to measure the quantity of *p*-nitrophenol released during the reaction. Each experiment was achieved in triplicates. The percentage inhibition was calculated using the equation: % inhibition = $(1 - A_{sample}/A_{control}) \times 100$, where a sample is the absorbance of the tested samples and $A_{control}$ is the absorbance of control. The $IC_{50}$ value was specified as the concentration of lipase inhibitor to inhibit 50% of its activity under the assay requirements.

## *In Vivo* Assay

### Body Weight Assessment

Due to insufficient amounts of the two major isoflavones (**2** and **5**), the extract was only evaluated for the *in vivo* assessment. A diet-induced obese rat model was obtained from the animal house in the National Research Centre. Fifteen Wistar rats (140–150 g) were held with a 12:12-h light-dark cycle in a temperature-controlled room. The diets provide at least 3.85 kcal/g of energy. The high-fat diet (HFD) was achieved by modifying the percentage of fat higher than a normal diet. Fat content is 20% sheep tallow and 1% cholesterol. Nipples of stainless steel for feeders and drinking were supplied for each cage to allow recording the individual feed intake of each rat. They were classified into three groups ($n = 5$) as follows: control group, received a normal chow diet (ND) for 8 weeks; group 1, received a HFD for 8 weeks; and group 2, received HFD + *T. resupinatum* extract (25 mg/kg body weight suspended in 0.5 ml saline) daily for 8 weeks by oral gavage. Body weight measurements were recorded from all groups at 0 and after 8 weeks.

### Blood Biochemical Analysis

Blood samples were taken by puncture of the rat orbital sinus. The samples were kept coagulating at room temperature for 20–30 min and then centrifuged at $1006 \times g$ for 15 min. Sera were separated and stored at 8 °C for biochemical analysis. Blood glucose levels were measured using the hexokinase colorimetric method. Triacylglycerides and total cholesterol levels were determined by enzymatic methods in all groups.

## Statistical Assessment

The data were produced as mean ± SD. Statistical assessment of the biochemical data was performed with SPSS software version 15. The comparison between group means was analyzed by one-way ANOVA.

## Molecular Docking

### Protein Structure Preparation

The prerequisite protein structure in the docking analyses was downloaded from PDB, http://www.rcsb.org.pdb (the Protein Data Bank). The crystal structure of the porcine lipase (PDB ID: 1ETH) was retrieved in PDB format. In the AutoDock tools, the structure was prepared by the exclusion of water molecules, and all heteroatom coordinates, added with missed atoms, polar hydrogens, and charges. It was made sure that no residues carry the non-integral charges which are a prerequisite for the receptor file in the software AutoDock 1.5.7 (Akshatha et al. 2021). Finally, the resulting protein file was saved as a PDBQT format.

### Ligand Preparation

The chemical structures of isolated constituents were obtained from the PubChem compound database (https://pubchem.ncbi.nlm.nih.gov) and retrieved as Structure Data File (SDF) formats. Compound **4** is unavailable on PubChem database; thus, it was sketched using ChemDraw (Cambridge Soft, Waltham, MA, USA) and further optimized and converted using Avogadro 1.2.0 (http://avogadro.cc/) to pdb files. Using AutoDock Tools software (version 1.5.7), the pdb files of the isolated chemicals were transformed into pdbqt files format (Swargiary and Daimari 2020). Orlistat, a medication used to treat obesity, was used as a positive control for molecular docking assay, downloaded through https://www.drugbank.ca/ (the drug bank website) and employed as acquired.

### Docking

After the preparation of ligands and protein, docking was accomplished in AutoDock Vina. We noted the *x*, *y*, *z* values

from attributes of the SBD site sphere using Biovia Discovery Studio software (v21.1, 2021) (Suryanarayana et al. 2021). A Search Space performed approximately the same size as pancreatic lipase, 60 Å radius was created and centered at $x = 71.52$, $y = 26.883$, $z = 187.849$ (Urbizo-Reyes et al. 2022), therefore, the set exhaustiveness parameter is increased. Separately, the individual ligand was docked with the enzymes and the final binding affinity (kcal/mol) of a given ligand-enzyme interaction was obtained. The docking binding between docked agents and the targets was analyzed using Biovia Discovery Studio software (v21.1, 2021) (Swargiary and Daimari 2020).

### ADME and Drug-Likeness Estimation

Website http://www.swissadme.ch was accessed in a web browser that displays the submission page of SwissADME and the canonical SMILES of the isolated phytoconstituents were input for estimation of ADME and drug likeness. The SwissADME server includes configurations which are selected for robustness, speed, and clear interpretation of the results. In addition, isolated compounds were subjected to molecular properties prediction for drug-likeness by MolSoft (MolSoft, 2007) software (Youssef et al. 2020).

## Results and Discussion

### Chemical Analysis

#### Isolation and Structure Elucidation

The applied chromatographic techniques managed the isolation of 14 phenolic compounds from *T. resupinatum* extract. Chemical and physical investigations were used to elucidate their structural composition. In addition, their structural data were compared with previously reported spectroscopic data for more confirmation. In addition to one phenolic acid (chlorogenic acid; **1**), three isoflavone aglycones: formononetin (**2**), pseudobaptigenin (**5**), and genistein (**7**); five isoflavone 7-*O*-β-glucosides; ononin (**3**; formononetin 7-*O*-β-glucoside), rothindin (**6**; pseudobaptigenin 7-*O*-β-glucoside), genistin (**8**; genistein 7-*O*-β-glucoside), daidzin (**9**; daidzein 7-*O*-β-glucoside), and sissotrin (**10**; biochanin A 7-*O*-β-glucoside) as well as the acetyl derivative; 6"-*O*-acetyl ononin (**4**; formononetin 7-*O*-β-(6"-*O*-acetyl) glucoside) were established. Furthermore, flavonol aglycones and their 3-*O*-β-glucoside; kaempferol (**11**), astragalin (**12**; kaempferol 3-*O*-β-glucoside), quercetin (**13**), and isoquercetin (**14**; quercetin 3-*O*-β-glucoside) were isolated. Compounds **4**, **8**, **9**, **10**, and **12** were isolated for the first time from *T. resupinatum* but reported beforehand for other *Trifolium* species. The physical constants and NMR data were compared with published values for all isolated compounds (see, Supporting Information).

#### LC-MS Profiling

Analysis of the LC-ESI-MS base peak chromatogram of the 70% aqueous methanol leaf extract of *T. resupinatum* (Fig. S1) revealed the dominance of pseudobaptigenin (peak 72, isolate **5**) and formononetin (peak 73, isolate **2**), and their respective 7-*O*-glucosides (peaks 57 and 58, isolates **6** and **3**, respectively). After ingestion, isoflavone glycosides are metabolized by the β-glucosidase enzyme in the small intestine to produce the more efficiently absorbed form of isoflavones with lower hydrophilic properties and smaller molecular weights (corresponding aglycons)(Kassem et al. 2017). Therefore, the two isoflavone aglycones **2** and **5** were selected for the *in vitro* pancreatic lipase assay along with the total extract.

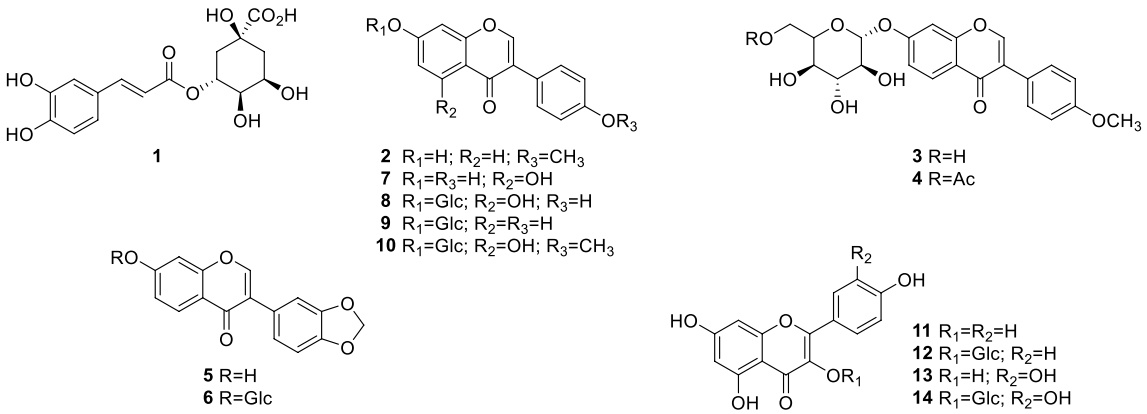

### Metabolite Annotation

In this context, detailed metabolite profiling of *T. resupinatum* leaf extract via HPLC-ESI-MS/MS was performed using a standard mixture including the isolated compounds (Fig. S1). For a more accurate representation of the species hydroalcoholic extract metabolome, molecular networking was created (Fig. 1). With the aid of GNPS libraries, possible correlations between each MS/MS spectrum were found, thereby enabling additional annotation of unknown but related molecules. About 81 metabolites were distinguished, 69 of which are species-first detection (Table S1). They belong to many chemical classes comprising fatty acids (four metabolites), amino acids (five metabolites), organic acids (two metabolites), and sugars (two metabolites) with phenolics as predominant class (68 compounds) (Fig. 2). The interpretated phenolics included 52 flavonoid compounds (23 isoflavonoids, 16 flavonols, seven flavones, five flavanones, and one flavanonol), along with 11 phenolic acids and aldehydes, as well as five coumarins (Table S1, Fig. 2).

In the negative ionization mode of the constructed molecular network, 425 nodes were grouped in 34 clusters (two linked nodes at least) and 191 self-looped nodes, whereby

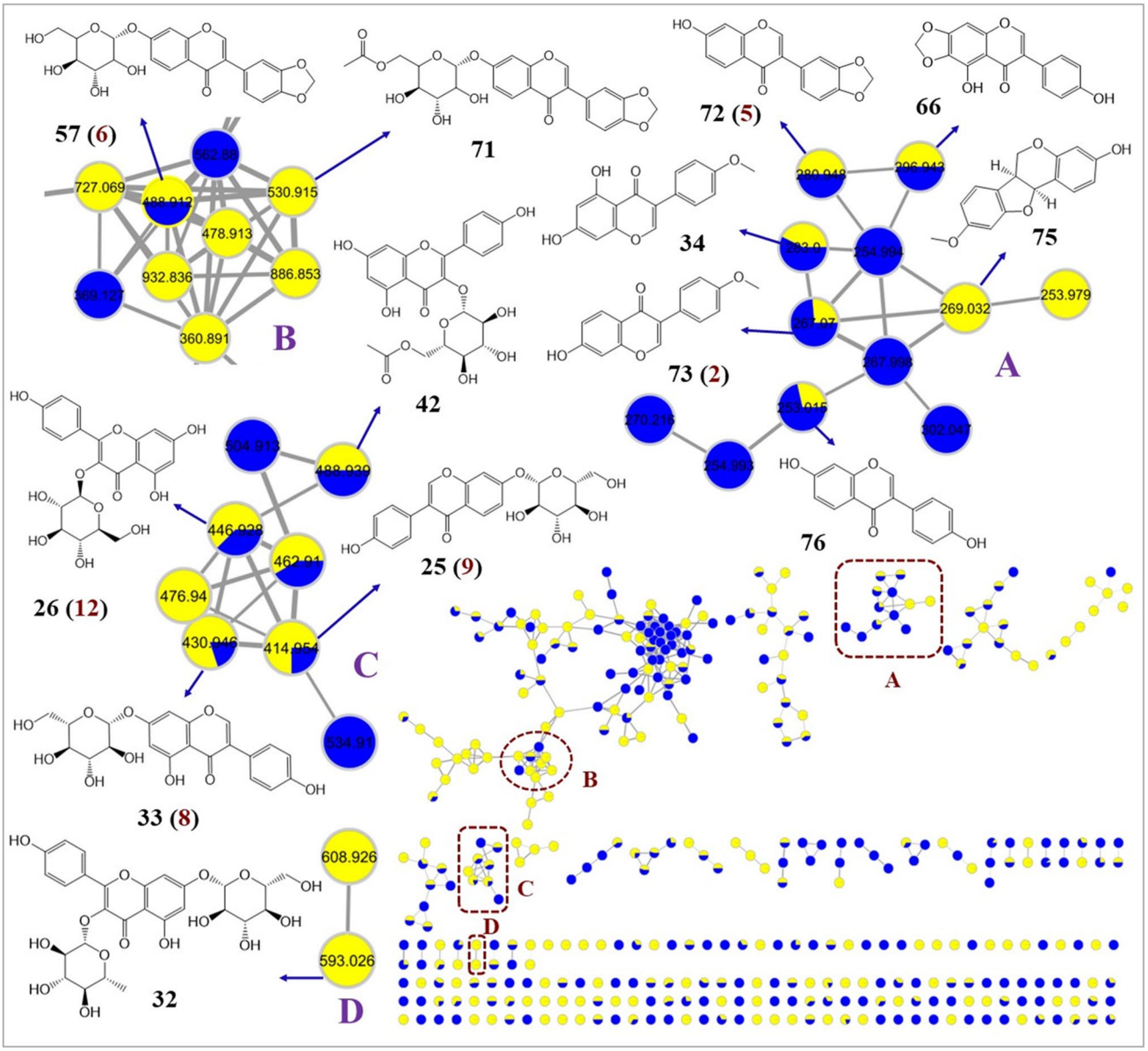


**Fig. 1** The molecular network created using MS/MS data (negative ionization mode) of *Trifolium resupinatum* extract (yellow) and standards mixture (blue)

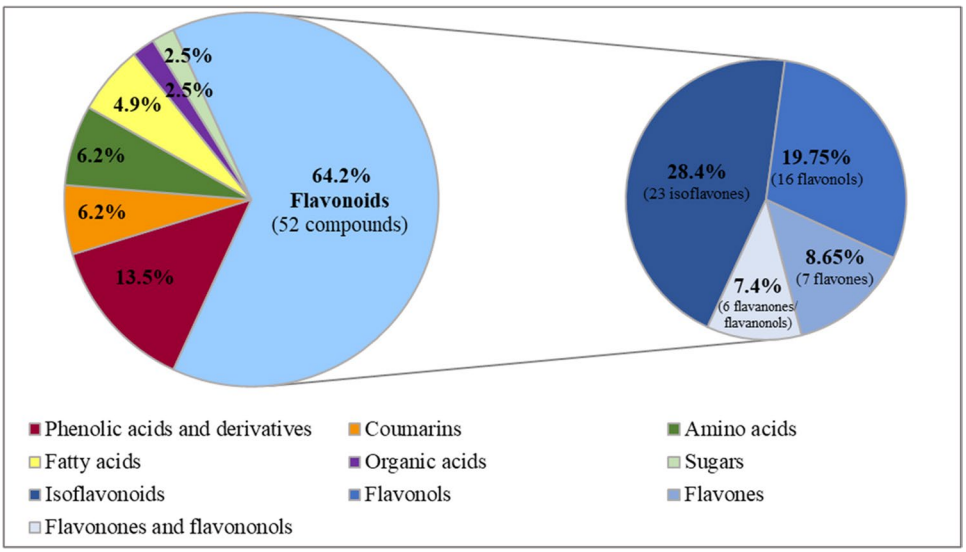


**Fig. 2** Classes of chemical metabolites identified in *Trifolium resupinatum* leaf extract with ratios of flavonoid subgroup structures in relation to the total of identified compounds

the interesting clusters A, B, C, and D guided the characterization of various phenolic skeletons (Fig. 1). The yellow nodes represent the targeted extract sample while the blue ones corresponded to the standards mixture ions. The unmatched clusters were analyzed and verified manually. On the other hand, the remaining constituents were tentatively elucidated via their accurate molecular weights, retention time, $MS^2$ fragments combined with GNPS libraries matches, and in parallel with the standards used or comparing their fragmentation picture with the previous reported data (Table S1).

Isoflavonoids are the most prominent constituents of the leguminous plant family (Fabaceae). They were frequently categorized into seven subclasses including isoflavones, isoflavans, isoflavanones, coumestans, rotenoids, pterocarpans, and coumaronochromones (Sohn et al. 2021). Members of the genus *Trifolium*, in particular red clover, contain significant concentrations of the variable structure patterns of the unique isoflavones in aglycone forms, daidzein (7,4′-dihydroxyisoflavone), genistein (4',5,7-trihydroxyisoflavone), formononetin (7-hydroxy-4´-methoxyisoflavone), biochanin A (5,7-dihydroxy-4′-methoxyisoflavone), and pseudobaptigenin (7-hydroxy-3',4'-methylenedioxyisoflavone), or some of their 7-glucoside forms, daidzin, genistin, ononin, sissotrin, and rothindin, respectively (Malca-Garcia et al. 2022). Less frequently occurring isoflavone aglycones such as prunetin (7-*O*-methyl-genistein), pratensein (3'-hydroxy biochanin A), and irilone (5,4'-dihydroxy-6,7-methylenedioxyisoflavone) have also been reported. In addition, minor acetylated and malonated glycosyl derivatives have been recorded (Das et al. 2020).

Cluster A of the created molecular network of *T. resupinatum* gathered 6 isoflavone aglycones encompassing nodes of formononetin (73, *m/z* 267.02 $[M-H]^-$) connected to biochanin A (34; *m/z* 283.01 $[M-H]^-$), and pseudobaptigenin (72; *m/z* 281.01 $[M-H]^-$) connected to irilone (66; *m/z* 297.01 $[M-H]^-$), both through the mass difference of 16 Da. Moreover, medicarpin (75; *m/z* 269.03 $[M-H]^-$) and daidzein (76; *m/z* 253.015 $[M-H]^-$) were grouped in the same cluster. Medicarpin is a benzopyran furanobenzene compound belonging to the pterocarpan phytoalexin group of the isoflavonoids family. It was formerly detected in several *Trifolium* species (Malca-Garcia et al. 2022) and various leguminous plants (Gampe et al. 2016; Cheng et al. 2019). Oxidation of pterocarpans yields coumestans which were also annotated in *T. pratense* and *T. repens* (Malca-Garcia et al. 2022). The most prevalent is coumestrol (54; *m/z* 267.02 $[M-H]^-$), which is perceived in *T. resupinatum* extract for the first time. It has an additional furan ring between B and C rings and dicatechol groups that resembles estradiol's structure to which its positive effects are attributed (Ionescu et al. 2021). Another set of six isoflavone aglycones were observed as self-looped nodes; hydroxy biochanin A (35; *m/z* 299.01 $[M-H]^-$), genistein (44; *m/z* 268.97 $[M-H]^-$), pratensein (51; *m/z* 299.01$[M-H]^-$), and prunetin (64; *m/z* 283.01 $[M-H]^-$), in addition to pseudobaptigenin-*O*-sulfate (60; *m/z* 360.98 $[M-H]^-$) monitored by the daughter ion peak at *m/z* 281 $[M-80]^-$ due to $SO_3$ loss. These compounds were not found in Persian clover beforehand except for isoflavone aglycones 34, 44, 71, 73, and 76.

Besides the isoflavonoid aglycones, some isoflavone glycosides were pictured in clusters B and C (Fig. 1). Pseudobaptigenin 7-*O*-glucoside (57; *m/z* 488.912 [M–H + FA (formic acid)]$^-$) is directly attached by a thick edge to 71 (*m/z* 530.91 $[M-H+FA]^-$) with a mass shift of 42 Da as probable acetyl moiety ($-COCH_3$), confirming the first identification of pseudobaptigenin 7-*O*-acetylglucoside in the genus *Trifolium*. On the other hand, both compounds appeared as formic acid adduct ions equivalent to $[M-H+HCOOH]^-$ or [M + 45 Da]$^-$, as compound 58

(formononetin 7-*O*-β-glucoside; *m/z* 474.93 [M–H + FA]$^-$). The isolated acetyl glucoside isomer of 58; acetylononin (45; *m/z* 471.03 [M−H]$^-$) was confirmed by the specific fragment at *m/z* 267 [M–H–acetyl−glucosyl]$^-$. The acetyl glycoside isoflavone conjugates of leguminous plants have already been mentioned (Gampe et al. 2016; Das et al. 2020); however, their presence in the studied species has not been previously reported. Furthermore, the characteristic ion of daidzin (25; *m/z* 414.96 [M−H]$^-$) was observed connected to that of genistin (33; *m/z* 430.94 [M−H]$^-$) in cluster C. Other glycosylated isoflavonoids were observed as self-looped nodes in the molecular network and could be annotated as coumestrol-*O*-hexoside (12; *m/z* 429.01 [M−H]$^-$), sissotrin (29; *m/z* 445.01 [M−H]$^-$), irilone-4′-*O*-glucoside (31; *m/z* 458.97 [M−H]$^-$), pratensein-*O*-glucoside (52; *m/z* 461.01 [M−H]$^-$), and dimethoxy isoflavone-*O*-hexoside (wistin) (63; *m/z* 505.01 [M–H + FA]$^-$) designated through the prominent peaks of their precursors' fragment ions due to loss of the hexoside moiety [M–H–162]$^-$. Numerous peaks were verified by comparing their mass spectra and retention data with those of standards, including the isolated compounds (Table S1). Previous studies characterized these isoflavone glycosides combinations in *T. pratense* (Malca-Garcia et al. 2022) and other leguminous species (Gampe et al. 2016; Cheng et al. 2019). However, our study is the first to dereplicate them in *T. resupinatum* except for compounds 33, 57, and 58.

An additional sulfated compound was recognized as a flavone structure and recognized as apigenin-*O*-sulfate (18; *m/z* 348.99 [M−H]$^-$). Other flavone aglycones were reported before in some *Trifolium* species (Malca-Garcia et al. 2022) and identified as apigenin (46; *m/z* 269.02 [M−H]$^-$), tricin (49; *m/z* 329.01 [M−H]$^-$), and chrysoeriol (69; *m/z* 299.01 [M−H]$^-$) confirmed by standard samples. The substitution with methoxy groups was indicated by the $(CH_2)_n$ subsequent loss $(-14\ Da)_n$ (Hussein et al. 2018). Apigenin 7-*O*-glucoside (30; *m/z* 431.01 [M−H]$^-$), apiin (40; *m/z* 562.96 [M−H]$^-$), and tricin 7-*O*-glucoside (37; *m/z* 491.01 [M−H]$^-$) were eluted earlier than their corresponding aglycones. Their annotation was supported by the elimination of the hexose [M–H−162]$^-$ or pentose [M–H−132]$^-$ moieties to produce the analogous aglycone anions.

Another acetyl derivative was also detected in cluster C concerning a mono-glycosyl flavonol structure, kaempferol 3-*O*-(6"-acetyl) glucoside (42; *m/z* 488.94 [M−H]$^-$) which is directly linked to a node at *m/z* 446.93 with 42 Da mass difference, that displayed kaempferol 3-*O*-glucoside (26; *m/z* 446.93 [M−H]$^-$) based on the standard isolated compound (Fig. 1). Meanwhile, this node was directly connected with its congeners; quercetin 3-*O*-glucoside (22; *m/z* 462.96 [M−H]$^-$) and isorhamnetin 3-*O*-glucoside (28; *m/z* 476.93 [M−H]$^-$) (Fig. 1). Other peaks sharing the same parent ions of 26 and 28 corresponded to kaempferol 7-*O*-glucoside (36; *m/z* 446.93 [M−H]$^-$) and isorhamnetin 7-*O*-glucoside (61; *m/z* 477.01 [M−H]$^-$) relying on the base peak ions [Agl−H]$^-$ at *m/z* 285 and 315, respectively. In contrast, these ions of the 3-*O*-isomers were [Agl−$H_2$]$^-$ at *m/z* 284 and 314 (Farid et al. 2022). The flavonol glycosides were also eluted first followed by their corresponding aglycones: kaempferol (50; *m/z* 285.01 [M−H]$^-$), quercetin (39; *m/z* 300.97 [M−H]$^-$), isorhamnetin (62; *m/z* 315.1 [M−H]$^-$), in addition to myricetin (67; *m/z* 317.02 [M−H]$^-$) that reported before in *T. repens* (Agraharam et al. 2022). Flavonols in the genus *Trifolium* are frequent, mainly kaempferol and quercetin (Malca-Garcia et al. 2022). They were stated earlier in the aerial parts of *T. resupinatum* (Kassem et al. 2017); however, the levels of different glycosylation and positional isomers are distinguished in the current study through the key fragmentation pathway approach. Two di-*O*-glycosyl flavonols appeared as a cluster (D) of two connected nodes representing quercetin 3-*O*-glucoside-7-*O*-rhamnoside (21; *m/z* 608.98 [M−H]$^-$) and kaempferol 3-*O*-glucoside-7-*O*-rhamnoside (32; *m/z* 593.02 [M−H]$^-$), further confirmed throughout the GNPS libraries. They produced diagnostic fragment ions at (*m/z* 463 [M–H–146]$^-$ and 447 [M–H−162]$^-$) and (*m/z* 447 [M–H−146]$^-$ and 431 [M–H−162]$^-$), respectively. The higher intensities for their glucosylated fragment ions [M–H+162]$^-$ than those for the rhamnosylated ones [M–H + 146]$^-$ suggested the substitution at 3-*O*-glucoside and 7-*O*-rhamnoside for both compounds (Farid et al. 2022). Further flavonols-*O*-diglycosides were observed as self-looped nodes and identified as 3-*O*-rutinoside of quercetin (24; *m/z* 609.01 [M−H]$^-$) and kaempferol (27; *m/z* 592.94 [M−H]$^-$). The last isomer was kaempferol 3,7 di-*O*-rhamnoside (38; *m/z* 577.01 [M−H]$^-$), which produced two diagnostic signals at *m/z* 431 [M–H−146]$^-$ and 285 [M–H−292]$^-$ compatible with the standard reference.

Limited amounts of other flavonoids rarely reported in the genus *Trifolium*, which correspond to flavanones and flavanonols, were obtained and observed in the molecular network as self-looped nodes. Two flavanone aglycones (47; *m/z* 255.01 [M−H]$^-$) and (53; *m/z* 271.01 [M−H]$^-$) suggested to be liquiritigenin and naringenin as described in *Trifolium subterraneum* L. and *T. partense* L., respectively (Prati et al. 2007), were also confirmed via GNPS libraries (Table S1). Their corresponding glycosylated derivatives, liquiritoside (19; *m/z* 416.96 [M−H]$^-$) and naringenin 7-*O*-glucoside (55; *m/z* 433.01 [M−H]$^-$), were evidenced by the product ion [M–H−162]$^-$. A further flavanone aglycone was detected as eriodyctiol (70; *m/z* 287.01 [M−H]$^-$). In addition to a single flavanonol aglycone, taxifolin (20; *m/z* 303.04 [M−H]$^-$) which was confirmed through a standard compound and previously reported in *T. partense* (Prati et al. 2007). Excepting rutin (24), quercetin (39), and kaempferol (50), all annotated flavonols, flavanones, and flavanonol are non-previously reported metabolites in *T. resupinatum*.

Additional minor phenolic derivatives were marked as self-looped nodes and newly characterized in *T. resupinatum*. They relied on their ion mass spectra, retention times, and mass fragmentation profile aided with GNPS, published literature, and available authentic references. Phenolic acids; caffeic (4; *m/z* 179.01 $[M-H]^-$), sinapic (7; *m/z* 223.02 $[M-H]^-$), coumaric (10 and 14; *m/z* 163.01 $[M-H]^-$), gentisic (17; *m/z* 153.02 $[M-H]^-$), vanillic (23; *m/z* 167.01 $[M-H]^-$), ferulic (41; *m/z* 193.01 $[M-H]^-$), and chlorogenic (80; *m/z* 353.09 $[M-H]^-$) acids, phenolic benzaldehydes; *p*-hydroxy benzaldehyde (13; *m/z* 121.01 $[M-H]^-$) and trimethoxy benzaldehyde (59; *m/z* 195.09 $[M-H]^-$) as well as dihydrocoumaroyl-*O*-glucoside (81; *m/z* 327.22 $[M-H]^-$) were demonstrated. Chlorogenic acid was isolated before from the investigated species by Kassem et al. (2017), while the other phenolic acids and aldehydes were reported previously in *T. partense* (Prati et al. 2007).

Likewise, coumarins are also reported to occur in forage plants represented herein as hydroxy methyl coumarin (15; *m/z* 175.01 $[M-H]^-$), dihydroxycoumarin (68; *m/z* 177.01 $[M-H]^-$), trihydroxy coumarin (56; *m/z* 193.08 $[M-H]^-$), and dihydroxycoumarin-*O*-hexoside (43; *m/z* 339.02 $[M-H]^-$). Compound 68 was identified as esculetin (6,7-dihydroxycoumarin) confirmed through the standard compound, and was characterized before in *T. partense* (Vlaisavljević et al. 2017). Successively, compound 43 was elucidated as esculetin-*O*-glucoside via mass difference of 162 Da.

## Anti-obesity Potential

### Pancreatic Lipase Inhibition

Triacylglycerides are hydrolyzed by the pancreatic lipase enzyme into glycerol and fatty acids, aiding in their absorption in the intestine. Lipase inhibition is an effective strategy for preventing triglyceride absorption and obesity. Orlistat inhibits this enzyme professionally but with various harmful effects on the gastric, renal, endocrine, and nervous systems, impairing the other medications' efficacy (Ragheb et al. 2021). *T. resupinatum* extract exerted an *in vitro* inhibition impact on porcine pancreatic lipase inhibition with an $IC_{50}$ of 471.32 ± 0.8 µg/ml. Comparing the selected compounds, formononetin (**2**) ($IC_{50}$ of 47.2 ± 1.1 µg/ml) demonstrated potential enzyme inhibitory activity than pseudobaptigenin (**5**) ($IC_{50}$ of 112.8 ± 1.23 µg/ml) considering the efficiency of orlistat ($IC_{50}$ of 23.8 ± 0.64 µg/ml), as summarized in Table 1.

Many studies have shown that naturally occurring phenolics demonstrated multifunctional properties that can effectually prevent obesity and related metabolic disorders. They are described to regulate digestion and fatty acid oxidation, as well as carbohydrate and lipid metabolism by modulating the activity of digestive enzymes (Oliveira et al. 2022). Pancreatic lipase inhibitory action of some prospective isoflavones has previously been evaluated. Cardullo et al. (2021) proved that modification of formononetin by hydroxylation or bromination improved the *in vitro* enzyme inhibitory properties. On the other hand, Deng et al. (2020) suggested the inhibitory effect of ethyl acetate fraction of the fungus *Grifola frondose* (Dicks.) Gray was correlated to its rich content of pseudobaptigenin.

## *In Vivo* Evaluation

Data in Table 2 compared the final total body weight (g) among the control and other groups. They indicated that rats who received a high-fat diet (HFD) significantly increased their total body weight compared with those who received a normal diet (ND). There was significant weight loss in HFD rats treated with *T. resupinatum* extract (25 mg/kg body weight suspended in 0.5 ml saline) compared with those that received only HFD.Furthermore, the results in Table 2 demonstrated that glucose, triacylglycerides, and

**Table 1** Pancreatic lipase % inhibition of *Trifolium resupinatum* leaf extract and the major isolated isoflavone aglycones

| Sample (µg/ml) | Mean of pancreatic lipase inhibitory % ± S.D | | | |
|---|---|---|---|---|
| | Extract | Formononetin (2) | Pseudobaptigenin (5) | Orlistat |
| 1000 | 63.25 ± 1.5 | 82.17 ± 2.1 | 67.32 ± 2.1 | 93.25 ± 1.5 |
| 500 | 58.31 ± 1.5 | 74.28 ± 0.63 | 61.32 ± 0.63 | 86.35 ± 2.1 |
| 250 | 51.74 ± 0.92 | 66.20 ± 1.5 | 56.41 ± 1.5 | 80.12 ± 0.58 |
| 125 | 36.29 ± 1.2 | 61.38 ± 2.1 | 52.67 ± 2.1 | 65.34 ± 1.5 |
| 62.5 | 19.82 ± 0.73 | 58.35 ± 0.72 | 39.35 ± 0.72 | 60.35 ± 2.1 |
| 31.25 | 12.74 ± 1.3 | 41.32 ± 1.5 | 14.98 ± 1.5 | 54.36 ± 2.6 |
| 15.63 | 5.31 ± 1.7 | 19.98 ± 0.63 | 6.35 ± 0.63 | 45.25 ± 3.1 |
| 7.81 | 0 | 5.35 ± 1.2 | 0 | 29.31 ± 1.4 |
| 0 | 0 | 0 | 0 | 0 |
| $IC_{50}$ (µg/ml) | 471.32 ± 0.8 | 47.2 ± 1.1 | 112.8 ± 1.23 | 23.8 ± 0.64 |

Values are expressed as the mean ± SD. All determinations were carried out in a triplicate manner

total cholesterol levels significantly increased in the sera of rats that received HFD compared with those in a control group. At the same time, these parameters significantly decreased in the group treated with *T. resupinatum* extract compared to the untreated one (HFD). This potential could be related to flavonoids, particularly isoflavones (formononetin and pseudobaptigenin) that represent major constituents in *T. resupinatum* leaf extract (Fig. 2) or related to the synergetic interactions of the natural compounds (Liu et al. 2022).

The anti-obesity effects of flavonoids occur through the modulation of proteins, genes, and transcription factors that contribute to reduced lipogenesis, increased lipolysis, and energy expenditure, in addition to moderating inflammatory responses and suppressing oxidative stress (Oliveira et al. 2022). Due to various flavonoid compounds (64.2% of total identified compounds) and their structural variations (Fig. 2, Table S1), the effects varied considerably. Their anti-obesity properties include repressing adipogenesis and lipogenesis by lowering the inflammatory mediators, deactivating the immune cells, enhancing mitochondrial activity by promoting the antioxidant effects, decreasing lipid peroxidation, modifying fat metabolism, regulating apoptosis, and increasing energy consumption (Deng et al. 2020; Oza and Kulkarni 2020; Liu et al. 2022).

## Molecular Docking

Molecular docking was carried out to confirm the pancreatic lipase activity of the significant isolates (**2** and **5**) and predict the affinity of the additional isolated compounds to this enzyme, to which the synergetic effect of the anti-obesity property is attributed. Binding affinity evaluation is used to determine the strength of biomolecular interactions, which is crucial in determining the possibility of an interaction arising in a cell (Odoemelam et al. 2022). Table S2 summarizes the interactions between the amino acids and the ligands at the porcine pancreatic lipase (PPL) binding sites. Docking analysis applied to the PPL protein revealed that all the isolated constituents have better or analogous binding free energies to the control drug (orlistat). The binding affinity of orlistat on pancreatic lipase enzyme is found to be −8.2 kcal/mol. The strongest binding affinity (−9.9 kcal/mol) is afforded by compounds **5**, **7**, **11**, and **13**, followed by compounds **2** and **4** (−9.8 kcal/mol), then compound **8** with a binding affinity −9.7 kcal/mol (Table S2). Our findings matched the docking results of Cardullo et al. (2021), who indicated the higher affinity of isoflavone class inhibitors to PPL active sites underlying their interactions. Also, it proved the better fitting of genistein (**7**) than formononetin (**2**) on the receptor due to the additional C-5 hydroxyl group which provides an additional hydrogen bond. Li et al. (2023) assumed the higher inhibitory effect of flavonols (quercetin) and isoflavones compared to flavanones and flavan-3-ols. Their inhibitory activity is enhanced by hydroxylation on rings A and B, whereas it is suppressed by glycosylation. In addition, Ahmed et al. (2022) showed a stronger affinity of chlorogenic acid to PPL active sites compared to orlistat.

Two- and three-dimensional illustrations of the interaction between ligand molecules and PPL protein are provided as supplementary material (Figs. S2 and S3). It was revealed from an analysis of docking interactions that all the isolated compounds bind to the same region as orlistat. Moreover, the observed interactions for the orlistat-PPL complex were close to those described in previous literature (de Lima Barros et al. 2022), which implies a good estimate of the present model.

The docking analysis displayed that His152 was involved in the hydrogen bonding interaction of orlistat, as compounds **1**, **4**, and **8** with the protein active site (Fig. S2 and S3). Additionally, it was found that both compound **11** and orlistat may stabilize the complex with the pancreatic lipase enzyme through a hydrogen bond with the same residue, Gly77 (Figs. S2 and S3). The similarity of the interacting pattern between these phytoconstituents and orlistat indicates that these isolated compounds probably inhibit pancreatic lipase in same pattern as orlistat. The top-scored inhibitors of phytoconstituents presented several π- interactions with Phe78, Tyr115, and Phe216 residues in a similar manner to the hydrophobic interaction of orlistat. A hydrophobic-interaction–based mechanism mainly triggers docking between compound **5** and PPL protein, where the pseudobaptigenin-PPL protein complex may be stabilized with 7 π- interactions. It

**Table 2** Effect of *Trifolium resupinatum* leaf extract on body weight, serum glucose, serum triacylglycerides, and total cholesterol (mg/dl) in HFD-treated rats

| Groups | Final body weight (g) | Serum biochemical parameters (mg/dl) | | |
|---|---|---|---|---|
| | | Glucose | Triacylglycerides | Total cholesterol |
| Control (ND) | 217 ± 18 | 114 ± 16 | 109 ± 9 | 83 ± 11 |
| Group 1 (HFD) | 260* ± 21 | 173* ± 26 | 142* ± 25 | 106* ± 10 |
| Group 2 (HFD + extract) | 245*# ± 13 | 120*# ± 16 | 79*# ± 10 | 85*# ± 13 |

The data is represented as mean ± SEM. The number of samples in each group = 5

*ND*, normal diet; *HFD*, high-fat diet

*Significantly different from ND. #Significantly different from HFD, all at $p < 0.05$

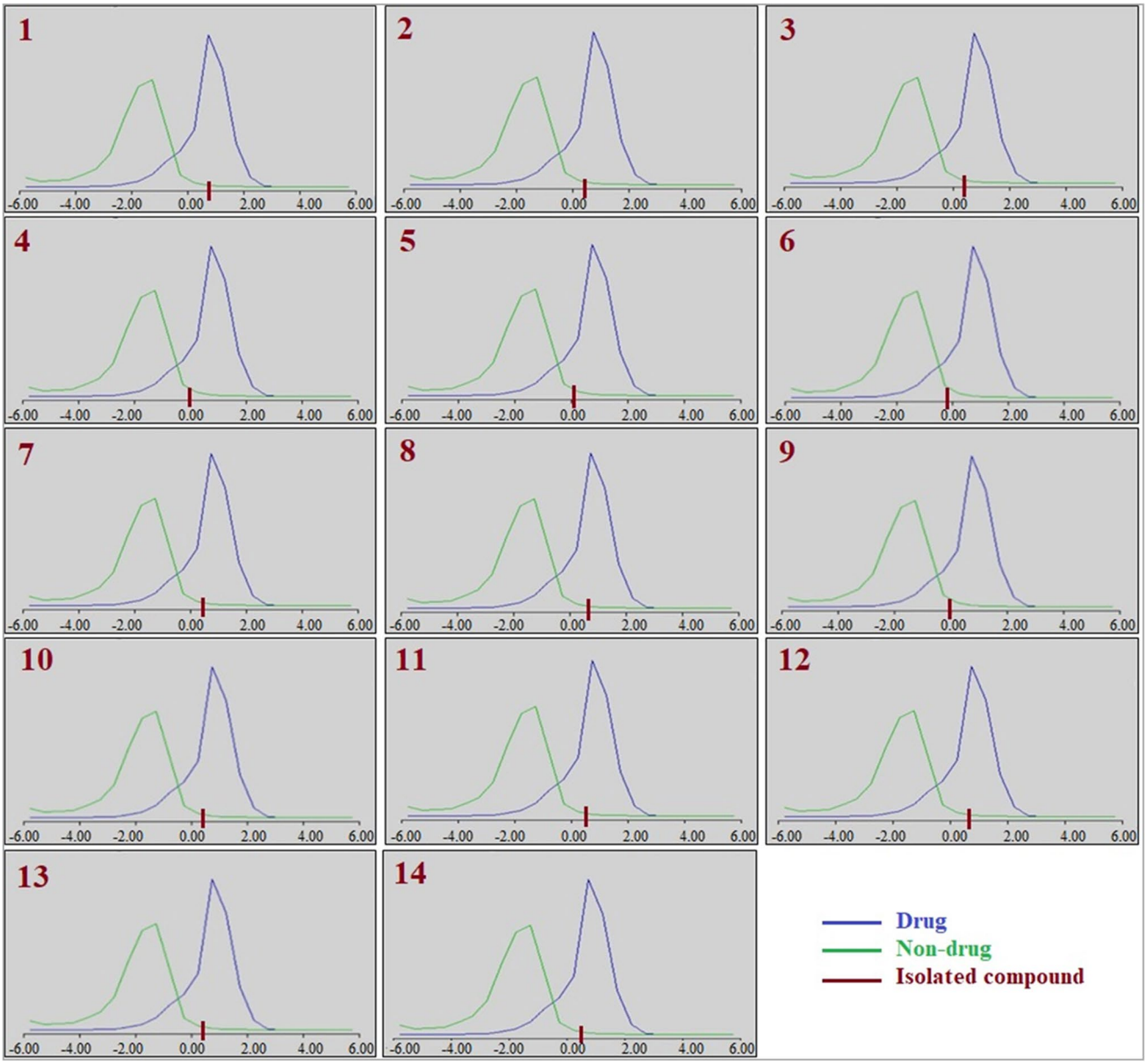


**Fig. 3** Plotting of drug-likeness score of isolated compounds using MolSoft. Green-colored curve is non-drug–like behavior and the blue-colored curve is drug-like behavior. Compounds with zero or negative values seem not to be drug candidates. DS, drug-likeness score; (**1**) chlorogenic acid, (**2**) formononetin, (**3**) ononin, (**4**) 6"-*O*-acetyl ononin, (**5**) pseudobaptigenin, (**6**) rothindin, (**7**) genistein, (**8**) genistin, (**9**) daidzin, (**10**) sissotrin, (**11**) kaempferol, (**12**) astragalin, (**13**) quercetin, (**14**) isoquercetin

was implied from previous literature that interaction with His264 is a key element since this residue constitutes the catalytic triad of the PPL active sites (de Lima Barros et al. 2022). Almost all the highly scored constituents formed a hydrophobic interaction with the key residue His264 (Fig. S2 and S3).

## Drug-Likeness and Oral Bioavailability

A detailed analysis of the pharmacokinetic properties of the isolated metabolites was performed. Lipinski specified a rule of five (RO5) to predict compounds that could be good drug candidates or drug-like compounds. The RO5 specified that poor absorption or permeation is more probable when there are more than five H-bond donors (HBD), molecular weight (MW) is over 50, Log *P* is over 5, and the sum of *N*'s and *O*'s (HBA) is over 10 (Abdul-Hammed et al. 2021).

As presented in Table S3, the HBD, MW, HBA, and Log *P* values of most isolated compounds obey the specifications of the RO5. Compounds **1** and **8** have one acceptable violation, as an orally active drug has no more than one violation of the Lipinski criteria (Ivanović et al. 2020). On the other hand, compounds **12** and **14** showed two violations. The bioavailability score aims to predict the possibility of a compound having at least 10% oral bioavailability in rats. The predicted bioavailability of the isolated compounds (Table S3) revealed a bioavailability score of 0.11, 0.17, or 0.55, which means good pharmacokinetic properties and good drug profile (Swain and Hussain 2022).

Distinctive to SwissADME is the bioavailability radar that provides a graphical preliminary glimpse at the drug-likeness parameters of the studied compounds. Figure S4 shows the drug-likeness graph as a hexagon, with each vertex indicating a characteristic that defines a bioavailable drug. The pink zone within the radar hexagon represents the optimal physicochemical space for each property predicted to be orally bioavailable (lipophilicity, XLOGP3 between −0.7 and + 5.0; size, MW between 150 and 500 g/mol; polarity, TPSA between 20 and 130 $Å^2$; solubility, log S not higher than 6; saturation, fraction of carbons in the sp3 hybridization not less than 0.25; and flexibility, no more than nine rotatable bonds) (Ndombera et al. 2019). Most of the constituents fall within the five parameters of the pink area and are considered drug-like.

According to the Molsoft database tool, the scale of a drug-likeness score of isolated compounds ranges from –0.15 to 0.79 (Fig. 3). The isolated compounds, which represent drug-likeness scores with positive values, are to be considered like drugs. On the contrary, compounds **4**, **6**, and **9** showed negative values, indicating low probabilities of being drugs (Gad et al. 2020).

## Conclusion

The chemical study of *T. resupinatum* leaf extract detected 81 metabolites, including 14 phenolic isolates, 69 of which were annotated for the first time in Persian clover. Two major isolated aglycones (formononetin and pseudobaptigenin) showed promising *in vitro* pancreatic lipase inhibitory actions, which might serve as a potential mechanism for anti-obesity. Preliminary *in vivo* screening on high-fat diet-induced obese rats showed that administration of the extract resulted in their weight loss and possible improvement of lipid serum triacylglycerides, total cholesterol, and glucose levels. The *in silico* investigation corroborated these findings and agreed to understand how these constituents interact with vital enzymes associated with obesity. It also granted them insights into the drug-likeness and ADME properties.

**Supplementary Information** The online version contains supplementary material available at https://doi.org/10.1007/s43450-023-00501-8.

**Acknowledgements** The authors thank the National Research Centre for supplying the facilities for this research.

**Author Contribution** MESK: conceptualization, resources, experimental (extraction, fractionation, isolation, structure elucidation), and review. MMM: conceptualization, experimental (software, NMR and LC–MS/MS processing, structure elucidation), resources (authentic standards), writing the original draft, review, and editing. AYR: conceptualization, experimental (isolation, NMR analysis, structure elucidation), writing original draft, review, and editing. NAR: conceptualization, experimental (software, networking, in silico investigation), writing original draft, review, and editing. EMY: conceptualization, experimental (*in vivo* biology), writing and review. EME: experimental (extraction, fractionation, and isolation), writing original draft, review. IAE: collection and identification of plant species. The final published version of the manuscript has been read and approved by all the authors.

**Funding** Open access funding provided by The Science, Technology & Innovation Funding Authority (STDF) in cooperation with The Egyptian Knowledge Bank (EKB).

**Data Availability** Data supporting the current study are available from the corresponding author upon reasonable request.

## Declarations

**Ethics Approval** The animal investigational procedure was declared by the Medical Research Ethics Committee of the National Research Centre (no. 04410623). Animal experimentation was performed according to national and institutional guidelines for animal care.



## References

Abdul-Hammed M, Adedotun IO, Falade VA, Adepoju AJ, Olasupo SB, Akinboade MW (2021) Target-based drug discovery, ADMET profiling and bioactivity studies of antibiotics as potential inhibitors of SARS-CoV-2 main protease (Mpro). VirusDisease 32:642–656. https://doi.org/10.1007/s13337-021-00717-z

Agraharam G, Girigoswami A, Girigoswami K (2022) Myricetin: a multifunctional flavonol in biomedicine. Curr Pharmacol Reports 8:48–61. https://doi.org/10.1007/s40495-021-00269-2

Ahmed SA, Salau S, Khan A, Saeed M, Ul-Haq Z (2022) Inhibitive property of catechin and chlorogenic acid against human pancreatic lipase: molecular docking and molecular dynamics simulation

investigations. Adv J Chem Sect A 5:226–240. https://doi.org/10.22034/ajca.2022.338380.1311

Akshatha JV, SantoshKumar HS, Prakash HS, Nalini MS (2021) *In silico* docking studies of α-amylase inhibitors from the anti-diabetic plant *Leucas ciliata* Benth. and an endophyte, *Streptomyces longisporoflavus*. 3 Biotech 11:51. https://doi.org/10.1007/s13205-020-02547-0

Al-Karmalawy AA, Farid MM, Mostafa A, Ragheb AY, Mahmoud SH, Shehata M, Abo Shama NM, Gaballah M, Mostafa-Hedeab G, Marzouk MM (2021) Naturally available flavonoid aglycones as potential antiviral drug candidates against SARS-CoV-2. Molecules 26:6559. https://doi.org/10.3390/molecules26216559

Cardullo N, Muccilli V, Pulvirenti L, Tringali C (2021) Natural isoflavones and semisynthetic derivatives as pancreatic lipase inhibitors. J Nat Prod 84:654–665. https://doi.org/10.1021/acs.jnatprod.0c01387

Cheng M, Ding L, Kan H, Zhang H, Jiang B, Sun Y, Cao S, Li W, Koike K, Qiu F (2019) Isolation, structural elucidation and *in vitro* hepatoprotective activity of flavonoids from *Glycyrrhiza uralensis*. J Nat Med 73:847–854. https://doi.org/10.1007/s11418-019-01329-0

Das S, Sharangi AB, Egbuna C, Jeevanandam J, Ezzat SM, Adetunji CO, Tijjani H, Olisah MC, Patrick-Iwuanyanwu KC, Adetunji JB, Ifemeje JC, Akram M, Moboladji BM, Onyeike PC (2020) Health benefits of isoflavones found exclusively of plants of the Fabaceae family. In: Functional foods and nutraceuticals. Springer International Publishing, pp 473–508. https://doi.org/10.1007/978-3-030-42319-3

de Lima BA, de Lima EJSP, Faria JV, Acho LRD, Lima ES, Bezerra DP, Soares ER, de Lima BR, Costa EV, Pinheiro MLB, Bataglion GA, da Silva FMA, Cardozo NMD, Gonçalves JFC, Koolen HHF (2022) Cytotoxicity and lipase inhibition of essential oils from amazon annonaceae species. Chemistry 4:1208–1225. https://doi.org/10.3390/chemistry4040081

Deng J, Guo W, Guo J, Li Y, Zhou W, Lv W, Li L, Liu B, Xia G, Ni L, Rao P, Lv X (2020) Regulatory effects of a *Grifola frondosa* extract rich in pseudobaptigenin and cyanidin-3-*O*-xylosylrutinoside on glycolipid metabolism and the gut microbiota in high-fat diet-fed rats. J Funct Foods 75:104230. https://doi.org/10.1016/j.jff.2020.104230

El-Sherei MM, Ragheb AY, Mosharrafa SA, Marzouk MM, Kassem MES, Saleh NAM (2018) *Pterygota alata* (Roxb.) R. Br.: chemical constituents, anti-hyperglycemic effect and anti-oxidative stress in alloxan-induced diabetic rats. J Mater Environ Sci 9:245–255. https://doi.org/10.26872/jmes.2018.9.1.28

El Shabrawy MOA, Hosni HA, El Garf IA, Marzouk MM, Kawashty SA, Saleh NAM (2014) Flavonoids from *Allium myrianthum* boiss. Biochem Syst Ecol 56:125–128. https://doi.org/10.1016/j.bse.2014.05.015

Elkordy A, Elshikh O, Abdallah N (2019) Floristic diversity and vegetation analysis of riparian and aquatic plants of the canals in the Sohag Governorate. Egypt Bot Microbiol Dep Sohag Univ 25:81–95

Farid MM, Ibrahim FM, Ragheb AY, Mohammed RS, Hegazi NM, Shabrawy MOE, Kawashty SA, Marzouk MM (2022) Comprehensive phytochemical characterization of *Raphanus raphanistrum* L.: *in vitro* antioxidant and antihyperglycemic evaluation. Sci African 16:e01154. https://doi.org/10.1016/j.sciaf.2022.e01154

Gad EM, Nafie MS, Eltamany EH, Hammad MSAG, Barakat A, Barakat A, Boraei ATA (2020) Discovery of new apoptosis-inducing agents for breast cancer based on ethyl 2-amino-4,5,6,7-tetra hydrobenzo[b]thiophene-3-carboxylate: synthesis, *in vitro*, and *in vivo* activity evaluation. Molecules 25:1–26. https://doi.org/10.3390/molecules25112523

Gampe N, Darcsi A, Lohner S, Béni S, Kursinszki L (2016) Characterization and identification of isoflavonoid glycosides in the root of spiny restharrow (*Ononis spinosa* L.) by HPLC-QTOF-MS, HPLC-MS/MS and NMR. J Pharm Biomed Anal 123:74–81. https://doi.org/10.1016/j.jpba.2016.01.058

Hussein SR, Marzouk MM, Kassem MES, Abdel Latif RR, Mohammed RS (2017) Chemosystematic significance of flavonoids isolated from *Diplotaxis acris* (Brassicaceae) and related taxa. Nat Prod Res 31:347–350. https://doi.org/10.1080/14786419.2016.1226831

Hussein SR, Abdel Latif RR, Marzouk MM, Elkhateeb A, Mohammed RS, Soliman AA, Abdel-Hameed ESS (2018) Spectrometric analysis, phenolics isolation and cytotoxic activity of *Stipagrostis plumosa* (Family Poaceae). Chem Pap 72:29–37. https://doi.org/10.1007/s11696-017-0254-0

Ionescu VS, Popa A, Alexandru A, Manole E, Neagu M, Pop S (2021) Dietary phytoestrogens and their metabolites as epigenetic modulators with impact on human health. Antioxidants 10:1893. https://doi.org/10.3390/antiox10121893

Ivanović V, Rančić M, Arsić B, Pavlović A (2020) Lipinski's rule of five, famous extensions and famous exceptions. Pop Sci Artic 3:171–177

Jungbauer A, Medjakovic S (2014) Phytoestrogens and the metabolic syndrome. J Steroid Biochem Mol Biol 139:277–289. https://doi.org/10.1016/j.jsbmb.2012.12.009

Kassem MES, Marzouk MM, Mostafa AA, Khalil WKB, Booles HF (2017) Phenolic constituents of *Trifolium resupinatum* var. minus: protection against rosiglitazone induced osteoporosis in type 2 diabetic male rats. J Appl Pharm Sci 7:174–183. https://doi.org/10.7324/JAPS.2017.70530

Kim YS, Lee YM, Kim H, Kim J, Jang DS, Kim JH, Kim JS (2010) Anti-obesity effect of *Morus bombycis* root extract: anti-lipase activity and lipolytic effect. J Ethnopharmacol 130:621–624. https://doi.org/10.1016/j.jep.2010.05.053

Kolodziejczyk-Czepas J (2016) *Trifolium* species – the latest findings on chemical profile, ethnomedicinal use and pharmacological properties. J Pharm Pharmacol 68:845–861. https://doi.org/10.1111/jphp.12568

Li MM, Chen YT, Ruan JC, Wang WJ, Chen JG, Zhang QF (2023) Structure-activity relationship of dietary flavonoids on pancreatic lipase. Curr Res Food Sci 6:100424. https://doi.org/10.1016/j.crfs.2022.100424

Lillich FF, Imig JD, Proschak E (2021) Multi-target approaches in metabolic syndrome. Front Pharmacol 11:554961. https://doi.org/10.3389/fphar.2020.554961

Liu Y, Liu C, Kou X, Wang Y, Yu Y, Zhen N, Jiang J, Zhaxi P, Xue Z (2022) Synergistic hypolipidemic effects and mechanisms of phytochemicals: a review. Foods 11:2774. 10.3390/foods11182774

Malca-Garcia GR, Liu Y, Nikolić D, Friesen JB, Lankin DC, McAlpine JB, Chen SN, Pauli GF (2022) Investigation of red clover (*Trifolium pratense*) isoflavonoid residual complexity by off-line CCS-qHNMR. Fitoterapia 156:105016. https://doi.org/10.1016/j.fitote.2021.105016

Marzouk MM, Elkhateeb A, Ibrahim LF, Hussein SR, Kawashty SA (2012) Two cytotoxic coumarin glycosides from the aerial parts of *Diceratella elliptica* (DC.) Jonsell growing in Egypt. Rec Nat Prod 6:237–241

Ndombera F, Maiyoh G, Tuei V (2019) Pharmacokinetic, physicochemical and medicinal properties of *N*-glycoside anti-cancer agent more potent than 2-deoxy-D-glucose in lung cancer cells. J Pharm Pharmacol 7:133–147. https://doi.org/10.17265/2328-2150/2019.04.003

Noubiap JJ, Nansseu JR, Lontchi-Yimagou, E. Nkeck JR, Nyaga UF, Ngouo AT, Tounouga DN, Tianyi FL, Foka AJ, Ndoadoumgue AL, Bigna J (2022) Geographic distribution of metabolic syndrome and its components in the general adult population: a meta-analysis of global data from 28 million individuals. Diabetes Res Clin Pract 188:109924. https://doi.org/10.1016/j.diabres.2022.109924

Odoemelam CS, Hunter E, Simms J, Ahmad Z, Chang M-W, Percival B, Williams IH, Molinari M, Kamerlin SCL, Wilson PB (2022)

*In silico* ligand docking approaches to characterise the binding of known allosteric modulators to the glucagon-like peptide 1 receptor and prediction of ADME/Tox properties. Appl Biosci 1:143–162. https://doi.org/10.3390/applbiosci1020010

Oliveira et al, 2022 Oliveira AK, de Oliveira e Silva AM, Pereira RO, Santos AS, Barbosa Junior EV, Bezerra MT, Barreto RS, Quintans-Junior LJ, Quintans JS (2022) Anti-obesity properties and mechanism of action of flavonoids: a review. Crit Rev Food Sci Nutr 62:7827-7848. https://doi.org/10.1080/10408398.2021.1919051

Oza MJ, Kulkarni YA (2020) *Trifolium pratense* (red clover) improve sirt1 expression and glycogen content in high fat diet-streptozotocin induced type 2 diabetes in rats. Chem Biodivers 17:e2000019. https://doi.org/10.1002/cbdv.202000019

Prati S, Baravelli V, Fabbri D, Schwarzinger C, Brandolini V, Maletti A, Tedeschi P, Benvenuti S, Macchia M, Marotti I, Bonetti A, Catizone P, Dinelli G (2007) Composition and content of seed flavonoids in forage and grain legume crops. J Sep Sci 30:491–501. https://doi.org/10.1002/jssc.200600383

Ragheb AY, El-Shabrawy M, El-Sharawy RT, Elkhateeb A, Radwan RA, Abdel-Hameed ESS, Kassem MES (2021) Phenolics isolation and chemical profiling of *Livistona australis* (R.Br.) Mart. fruit extracts; potent inhibitors of α-amylase and pancreatic lipase. Trop J Nat Prod Res 5:272–280. https://doi.org/10.26538/tjnpr/v5i2.10

Sarma S, Sockalingam S, Dash S (2021) Obesity as a multisystem disease: trends in obesity rates and obesity-related complications. Diabetes Obes Metab 23:3–16. https://doi.org/10.1111/dom.14290

Singh T, Ramakrishnan S, Kumar Mahanta S, C. Tyagi V, Kumar Roy A (2019) Tropical forage legumes in india: status and scope for sustaining livestock production. In: Forage Groups, IntechOpen

Sohn SI, Pandian S, Oh YJ, Kang HJ, Cho WS, Cho YS (2021) Metabolic engineering of isoflavones: an updated overview. Front Plant Sci 12:670103. https://doi.org/10.3389/fpls.2021.670103

Suryanarayana K, Robert AR, Kerru N, Pooventhiran T, Thomas R, Maddila S, Jonnalagadda SB (2021) Design, synthesis, anticancer activity and molecular docking analysis of novel dinitrophenylpyrazole bearing 1,2,3-triazoles. J Mol Struct 1243:130865. https://doi.org/10.1016/j.molstruc.2021.130865

Swain SS, Hussain T (2022) Combined bioinformatics and combinatorial chemistry tools to locate drug-able anti-tb phytochemicals: a cost-effective platform for natural product-based drug discovery. Chem Biodivers 19:e202200267. https://doi.org/10.1002/cbdv.202200267

Swargiary A, Daimari M (2020) Identification of bioactive compounds by GC-MS and α-amylase and α-glucosidase inhibitory activity of *Rauvolfia tetraphylla* L. and *Oroxylum indicum* (L.) Kurz: an *in vitro* and *in silico* approach. Clin Phytosci 6:60:75. https://doi.org/10.1186/s40816-020-00219-3

Urbizo-Reyes U, Liceaga AM, Reddivari L, Kim KH, Anderson JM (2022) Enzyme kinetics, molecular docking, and *in silico* characterization of canary seed (*Phalaris canariensis* L.) peptides with ACE and pancreatic lipase inhibitory activity. J Funct Foods 88:104892. https://doi.org/10.1016/j.jff.2021.104892

Vlaisavljević S, Kaurinović B, Popović M, Vasiljević S (2017) Profile of phenolic compounds in *Trifolium pratense* L. extracts at different growth stages and their biological activities. Int J Food Prop 20:3090–3101. https://doi.org/10.1080/10942912.2016.1273235

Xu R, Lee J, Chen L, Zhu J (2021) Enhanced detection and annotation of small molecules in metabolomics using molecular-network-oriented parameter optimization. Mol Omi 17:665–676. https://doi.org/10.1039/d1mo00005e

Yokoyama SI, Kodera M, Hirai A, Nakada M, Ueno Y, Osawa T (2020) Red clover (*Trifolium pratense* L.) sprout prevents metabolic syndrome. J Nutr Sci Vitaminol 66:48–53. https://doi.org/10.3177/jnsv.66.48

Youssef E, El-Moneim MA, Fathalla W, Nafie MS (2020) Design, synthesis and antiproliferative activity of new amine, amino acid and dipeptide-coupled benzamides as potential sigma-1 receptor. J Iran Chem Soc 17:2515–2532. https://doi.org/10.1007/s13738-020-01947-6